ICRIE 2023 4th INTERNATIONAL CONFERENCE ON RECENT INNOVATIONS IN ENGINEERING

*Proceedings of the 4th International Conference on Recent Innovation in Engineering*
*ICRIE 2023, University of Duhok, College of Engineering, 13th – 14th September 2023*
*(Special issue for Passer journal of basic and applied sciences)*
*Paper No. 05*

# Reliability of Digital Image Correlation Techniques for Cementitious Composite Fracture Characterization

**[*] Haruna IBRAHIM[1] ,George WARDEH[1], Hanaa FARES[1]**
1, L2MGC, CY Cergy Paris University, 95031 Neuville-sur-Oise, France
* Corresponding author: haruna.ibrahim@etu.u-cergy.fr, Tel: +33749555983.
haruna.ibrahim@etu.u-cergy.fr; george.wardeh@cyu.fr; hanaa.fares@cyu.fr

## ABSTRACT

Conventional devices used for measuring strain, like strain gauges and LVDTs, typically used as single-point sensors, require enhanced precision of gathered data, encompassing accuracy and consistency. However, these instruments are incapable of generating strain maps. Furthermore, it requires more time and precision during the set-up test. However, this study assesses the reliability of digital image correlation (DIC) methods as a non-destructive and helpful tool for monitoring the development of cracks in cementitious composites by comparing the DIC test and the mechanical test (Machine test) results. In the objective study, three types of mortars were prepared: Normal Strength Mortar (NSM), High Strength Mortar (HSM), and High Strength Mortar with Fly Ash (HSMFA). Steel 13 mm in length and synthetic fibres 19mm and 54 mm in length (short and long) were mixed into the composites in varied volume ratios, ranging from 0% to 1. Pre-notched 40x40x160 mm prismatic specimens were tested in three-point bending while being simultaneously filmed to track the crack's growth. The results showed that the post-cracking behaviour switches from softening to hardening for some types of mortar and certain fibre dosages. To evaluate the reliability of DIC for the characterisation of fracture properties, the vertical displacements for all specimens were analysed using GOM correlate software and compared with machine test data. The use of the DIC approach for the measurement of crack opening and the interpretation of the results in terms of Force- crack mouth opening displacement (CMOD) were made possible by the good agreement between the results regarding vertical deflection for all the employed mortars.

**KEYWORDS:** Mortar; Fibres; Post Cracking Properties; Digital Image Correlation (DIC**)**

## 1 INTRODUCTION

Traditional strain measurement instruments commonly employed as point-wise sensors (PWS), such as strain gauges and LVDTs, need to improve the quality of information collected, i.e., data accuracy and reproducibility, and cannot provide strain maps[1]. Furthermore, the set-up test requires more time and precision. However, the Digital Image Correlation (DIC) technique, which falls under optical, non-interferometric methods, allows full-field strain measurements and is less time-consuming [2]. This method determines deformations by comparing images of the object's surface before and after deformation. The DIC techniques enable new and more complex investigations. The DIC technique was first introduced in the 1980s and has since seen significant advancements, with improved digital image quality and the implementation of several algorithm modifications. With high sensitivity and accuracy today, DIC is extensively used for testing specimens and entire structures [[3–10]]. DIC is a precise and non-contact optical method for measuring displacement and deformation in structural elements or materials under external loading[6]. It relies on the principles of continuum mechanics (rigid body mechanics) [5]. The

system primarily consists of digital cameras and specialised computer software, such as the Istra 4D program [3]. These cameras capture consecutive images of the object's surface before and during deformation, and the DIC software analyses this digital image data using mathematical correlation analysis. The result is a set of displacement and deformation maps for the entire surface of the specimen [8], which can also be used to evaluate stress fields based on the strain fields.

There are two forms of digital image correlation systems: a low-speed system and a high-speed one. It is possible to use the first mentioned only at low sampling frequencies (maximally several fps). Such a system mostly contains objectives with higher resolution, and thus, it is suitable for deformation analyses [8]

The DIC system's measurement of displacement/deformation requires the following consecutive stages.

- Preparation of the surface of specimens (Patterning)
- Calibration of a device according to the required procedure (using the DIC system calibration)
- Recording images of the examined object/material surface before and during its deformation
- Image analysis (evaluation) using a specialised computer program (software)
- visualisation of the results.

The main mechanical limitation of concrete arises from its limited ability to withstand tension and its deficiency in ductility. In some design procedures, its tensile strength is negligible. The failure of concrete under tension is attributed to micro-cracking at the interface between cement and aggregates, and the ability of these cracks to propagate under tensile loads explains its weakness. Therefore, the fracture properties of concrete are reported by examining its tensile behaviour after the initial crack has formed. Extensive research has focused on understanding different-sized specimens' crack formation, propagation, and behaviour under uniaxial or bending tests [11–18].

Reinforced Polymers (FRP) are currently used in concrete structural members as an alternative material to steel rebar because of their lightweight, high specific strength, ease of moulding, and excellent chemical and biological resistance [12]18, [19, 20,21]. Fibre is a small, discrete reinforcement material made from steel, glass, basalt, organic polymers (synthetic), and natural fibres with various shapes and sizes [12,22–24]

### 1.2 Principle of Digital Image Correlation Techniques

The basic principle of 2D Digital Image Correlation (DIC) involves tracing or matching identical points (pixels) between two images captured before and after deformation, as schematically illustrated in Figure 1.

A square reference subset centred around the coordinates of P ($x_0$, $y_0$) is chosen from the initial image to calculate the displacements of a specific point, denoted as P. This subset is then used to track the corresponding position of P in the deformed image. The reason for selecting a square subset rather than an individual pixel is that it contains a broader range of grayscale variations, enabling it to stand out from other subsets. This distinctiveness facilitates more accurate identification of the deformed image. The advantage of DIC lies in its accessibility, as it only requires basic equipment like a camera(s), a personal computer, and free image processing software[1][25–27]. The technique involves capturing images of a sample under external forces and subsequently applying image analysis to quantitatively derive displacement and strain information for materials [28]. DIC generates displacement data by comparing the positional differences of a Point of Interest (POI) using two images taken from the same location in a global coordinate system. Structural speckles must be applied to create variations in grayscale intensity across the specimen surface [29]. These speckles can either be the natural texture of the specimen's surface or, in some cases, artificially created by spraying black paint onto the white background of the specimen's surface. Alternatively, other techniques can be employed [2]. These speckles are used for image processing, comparing the deformed images against a reference image, which is assumed to be undeformed, to determine relative positions [26,28,29]. Illustrated in Figure 1, point P in its original position undergoes transformation to point P' after deformation. The coordinates of P' can be mathematically expressed [30].

Diagram depicting an initial square segment used as a reference, prior to any deformation, alongside a subsequent segment (referred to as "target" or "deformed"), following deformation as indicated in references [1,2].

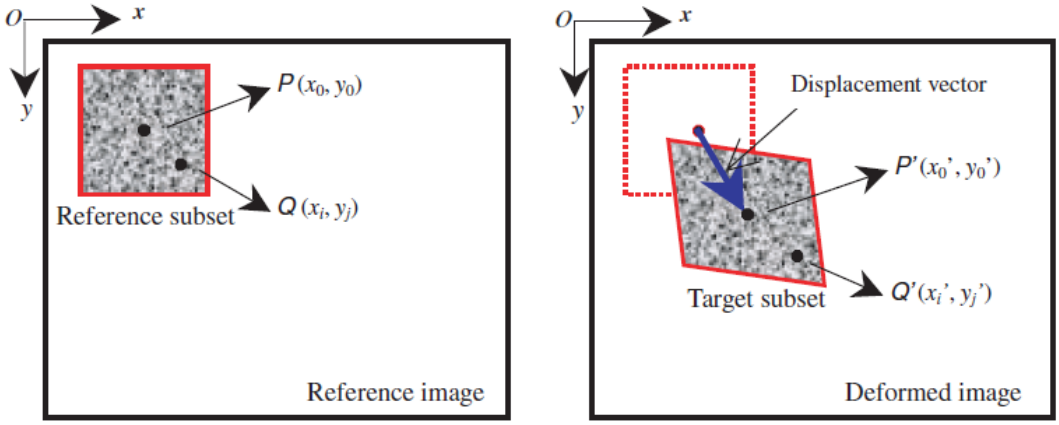


**Figure 1.** Diagram depicting a reference square subset before deformation and a target (or deformed) subset after deformation [1,2]

$$x' = x + u(x,y)$$
$$y' = y + v(x,y)$$

Equation 1

where $u(x,y)$, $v(x,y)$ are the horizontal and vertical displacements.

The non-deformed image is divided into finite sub-images, and the correlation coefficient (COF) between the two sub-images is given by equation 2. A value $COF = 1$ between the un-deformed sub-images A and the deformed sub-image B. This correlation means B is the same as A after deformation [27,29,31,32].

$$COF = \frac{\sum g_{ij} g_{ij}}{\sqrt{\sum g_{ij}^2 \sum g_{ij}^2}}$$

Equation 2

In equation 2, $g_{ij}$ and $\widehat{g_{ij}}$ Are the greyscale of image A on the coordinate $(i,j)$.

The deformation gradient, named $[F]$, which represents the derivative of each component of the deformed vector, $\vec{x}(x_1,x_2,x_3)$, for each component of the reference $\vec{X}(X_1,X_2,X_3)$ Vector is used to describe the displacement. $\vec{u}(X_1,X_2,X_3)$ [30].

$$[F] = \begin{bmatrix} \frac{\partial x_1}{\partial X_1} & \frac{\partial x_2}{\partial X_1} & \frac{\partial x_3}{\partial X_1} \\ \frac{\partial x_1}{\partial X_2} & \frac{\partial x_2}{\partial X_2} & \frac{\partial x_3}{\partial X_2} \\ \frac{\partial x_1}{\partial X_3} & \frac{\partial x_2}{\partial X_3} & \frac{\partial x_3}{\partial X_3} \end{bmatrix}$$

Equation 3

$$\vec{u} = \vec{x} - \vec{X} \Rightarrow [F] = [I] + \frac{\partial u}{\partial X}$$

Equation 4

with $[I]$ The unit matrix.

The Green strain tensor, $[E]$, is based on the deformation gradient as follows [30].

$$[E] = \frac{1}{2}\left([F]^T [F] - [I]\right)$$

Equation 5

## 2 METHODS

### 2.1 Materials used

Portland cement CEM I 52,5 N CE CP2 NF produced from the EQIOM factory in France [33] were used in this study. The cement properties are summarised in Table 1.

**Table 1.** Properties of the used cement.

| **CEM I 52,5 N CE CP2 NF** | | | | | | | | | |
|---|---|---|---|---|---|---|---|---|---|
| **Oxide (%)** | **$SiO_2$** | **$Al_2O_3$** | **$Fe_2O_3$** | **CaO** | **MgO** | **$SO_3$** | **$K_2O$** | **$Na_2O$** | **LOI** |
| | 18.6 | 5.6 | 4.1 | 63.9 | 1.92 | 2.4 | 0.82 | 0.44 | 1.35 |
| Clinker composition **(%)** | $C_3S$ | $C_2S$ | $C_3A$ | $C_4FA$ | - | - | - | - | - |
| | 67.0 | 9.0 | 8.4 | 11.4 | - | - | - | - | - |
| Density ($g/cm^3$) | 3.11 | | | | | | | | |
| Specific surface ($cm^2/g$) | 3950 | | | | | | | | |
| Compressive strength at two days (MPa) | 31.7 | | | | | | | | |

The lists of the properties of Class F fly ash utilised in this experiment, which was acquired from the French Ferrosil-icon factory, are shown in Table 2.

**Table 2**. Properties of the used fly ash

| Oxide | $SiO_2$ | $AlO_3$ | $FeO_3$ | CaO | MgO | $SO_3$ | $K_2O$ | $Na_2O$ | LOI |
|---|---|---|---|---|---|---|---|---|---|
| (%) | 58.6 | 23.3 | 6.4 | 3.4 | 0.5 | 0.3 | 1.1 | 0.38 | 3.0 |
| Density ($g/cm^3$) | 3.11 | | | | | | | | |
| Specific surface ($m^2/kg$) | 395 | | | | | | | | |
| Compressive strength (MPa) at 2 days | 31.7 | | | | | | | | |

For all mixing operations in this study, 0/4 mm washed semi-crushed sand was used. Sika discrete 5930L superplasticiser was employed. This superplasticiser has a solid content of 35% and is approved as a water-reducing additive, following the standard [34]

This study used three types of fibre: Sika Fibre Force 19mm, Sika Fibre Force 54 and micro steel fibre 13 mm (Figure 2 ). The shape of both synthetic fibre types is twisted multi-filament, the density is 0.92, the tensile strength is 689 MPa, and the elastic modulus is 5.57 GPa, according to the product data sheets. The first fibre, Sika Fibre Force 19, is 19 mm long and 0.34 mm in diameter and aspect ratio, which is defined by the length/diameter (L/D), 55.88 (Figure 2a), and It was referred to as short synthetic (SSYN) fibre in this study. Sika Fibre Force 54 is 54 mm long and 0.34 mm in diameter with an aspect ratio (L/D) of 158.8 and is referred to as long synthetic fibre (LSYN), as in Figure 2b. In the case of steel fibre, Bekaert company delivered the used copper-coated smooth microsteel fibre (SF), which is 13 mm long and 0.2 mm in diameter (Figure 2c). The aspect ratio of steel fibre (L/D) is 65, with a tensile strength of 2850 MPa. The fibres' properties are according to the manufacturer's product data sheet.

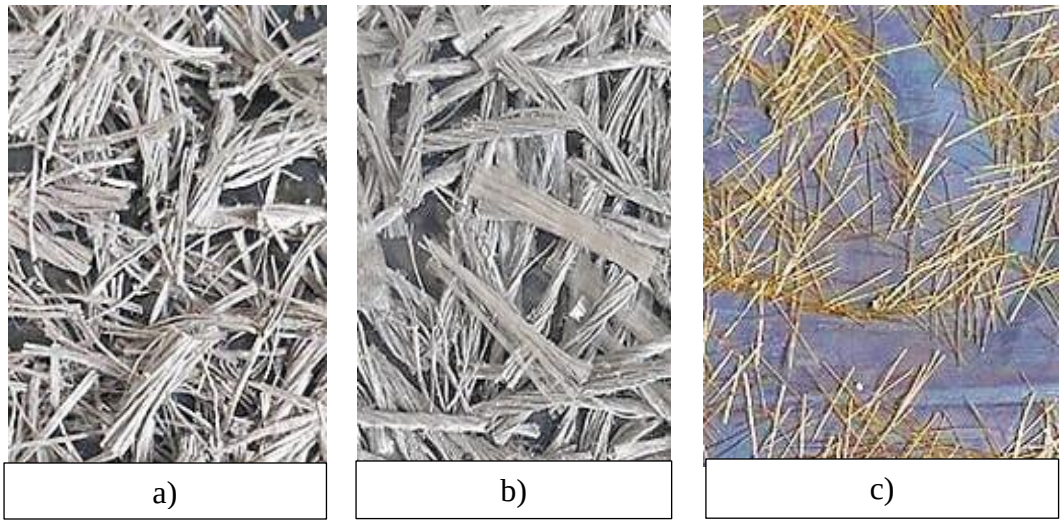


**Figure 2** a) Sika force 19 mm synthetic fibre b) Sika force 54 mm synthetic fibre c) Micro steel fibre.

## 2.2 Mix design method

The concrete equivalent mortar method replaces the gravel in the concrete formulation with sand that develops the same surface as the removed gravel. The technique was formed in early 2000 by Schwartzentruber and Catherine [28]. They found a linear correlation between the workability of concrete and mortar because the volume of water and the surface of solid components are preserved. The concrete vertical slump corresponds to a spread at the mortar scale of a diameter equal to the slump, as shown by many researchers [29,30] [31]. Concrete requires aggregates of sand and gravel for production to achieve the design strength. In this case, the concrete equivalent mortar method replaced the gravel volume with equal sand. It added with initial design (concrete mix design) volume to get a hint about the property at a small scale (mortar) before getting into concrete to save time and materials.

Three types of mortars were prepared: Normal Strength Mortar (NSM), High Strength Mortar (HSM), and High Strength Mortar with Fly Ash (HSMFA). Steel fibre (SF), short synthetic fibre (SSYN), and long synthetic fibres ( LSYN) were used. 0, 0.6, and 1.0 are the fibre dosages per cent of the total mortar's volume using a water-to-binder ratio of 0.5 for the NSM, 0.3 for the HSM, and 0.26 for the HSMFA (Table 3).

**Table 3.** Mix design proportions of the Mortars for $1m^{3.}$

| Specimens **Identification** | Materials | | | | | |
|---|---|---|---|---|---|---|
| | **Cement ($kg/m^3$)** | **Fly ash ($kg/m^3$)** | **Water ($kg/m^3$)** | **Sand ($kg/m^3$)** | **Fibre ($kg/m^3$)** | **Superplasti-ciser ($kg/m^3$)** |
| NSM (Reference) | 577 | - | 289 | 1251 | - | 4.4 |
| HSM (Reference) | 757 | - | 227 | 1208 | - | 27 |
| HSMFA (Reference) | 701 | 73 | 233 | 1131 | - | 38 |
| NSM_SSYN_0.6 | 578 | - | 288 | 1236 | 6 | 4.6 |
| NSM_SSYN_1.0 | 576 | - | 288 | 1230 | 9 | 4.6 |
| NSM_LSYN_0.6 | 578 | - | 288 | 1236 | 6 | 4.6 |
| NSM_LSYN_1.0 | 576 | - | 288 | 1230 | 9 | 4.6 |
| NSM_SF_0.6 | 576 | - | 288 | 1237 | 45 | 4.9 |
| NSM_SF_0.8 | 575 | - | 288 | 1235 | 61 | 4.9 |
| HSM_SSYN_0.6 | 753 | - | 226 | 1195 | 6 | 28 |

| | | | | | | |
|---|---|---|---|---|---|---|
| HSM_SSYN_1.0 | 750 | - | 225 | 1191 | 9 | 32 |
| HSM_LSYN_0.6 | 753 | - | 226 | 1195 | 6 | 28 |
| HSM_LSYN_1.0 | 750 | - | 225 | 1191 | 9 | 32 |
| HSM_SF_0.6 | 737 | - | 221 | 1172 | 45 | 35 |
| HSM_SF_0.8 | 731 | - | 219 | 1159 | 66 | 49 |
| HSMFA_SSYN_0.6 | 710 | 76 | 206 | 1180 | 6 | 28 |
| HSMFA SSYN_1.0 | 708 | 75 | 206 | 1171 | 9 | 32 |
| HSMFA_LSYN_0.6 | 710 | 76 | 206 | 1180 | 6 | 28 |
| HSMFA_LSYN_1.0 | 708 | 75 | 206 | 1171 | 6 | 32 |
| HSMFA_SF_0.6 | 710 | 76 | 206 | 1180 | 6 | 28 |
| HSMFA_SF_0.8 | 708 | 75 | 206 | 1171 | 6 | 32 |

## 2.3 Experimental test

In the present work, twenty-one series of mortars were derived from mixtures. The mortar's horizontal flow is measured using a mini cone whose dimensions are deduced from Abram's cone by a homothetic ratio of two, as in Table 4. The upper diameter of the cone is 50 mm, the lower diameter is 100 mm, and the height is 150 mm, as in Figure 3. The mortar mixture was poured into a 40 x 40 x 160 mm prism plastic mould and allowed to cure in water for 28 days at 20° C.

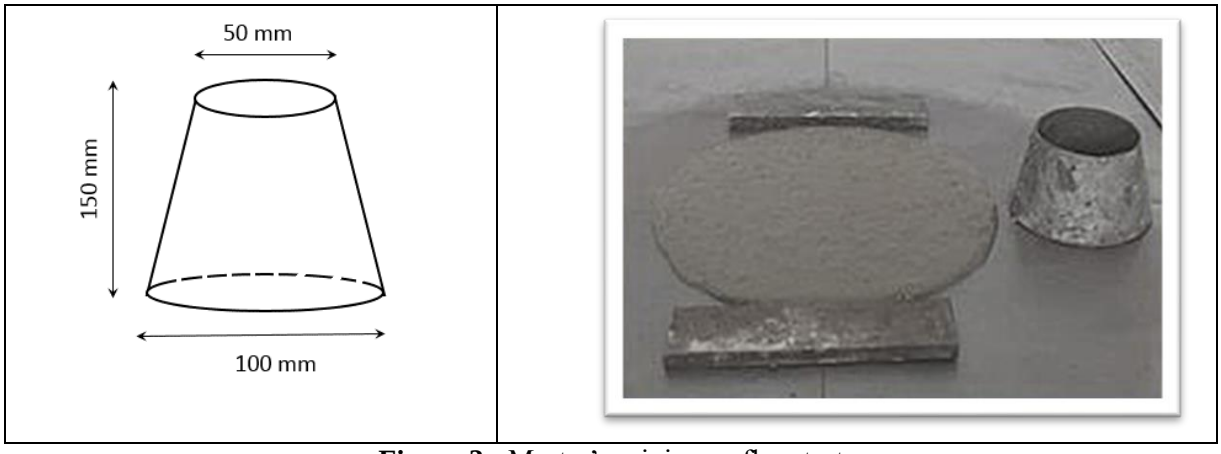


**Figure 3:** Mortar's mini cone flow test

Table 4. Mortar's flow test

| Specimens Identification | Superplastiser (% of binder) | Flow (mm) |
|---|---|---|
| NSM (Reference) | 0.75 | 345 ± 3.3 |
| HSM (Reference) | 4.0 | 352 ± 2.5 |
| HSMFA (Reference) | 5.0 | 346 ± 3.8 |
| NSM_SSYN_0.6 | 0.8 | 351 ± 3.2 |
| NSM_SSYN_1.0 | 0.8 | 340 ± 2.7 |
| NSM_LSYN_0.6 | 0.85 | 345 ± 3.4 |
| NSM_LSYN_1.0 | 0.85 | 338 ± 2.0 |
| NSM_SF_0.6 | 0.85 | 341 ± 2.3 |

| | | |
|---|---|---|
| NSM_SF_0.8 | 0.85 | 339 ± 1.1 |
| HSM_SSYN_0.6 | 4.0 | 342 ± 2.6 |
| HSM_SSYN_1.0 | 4.4 | 348 ± 1.5 |
| HSM_LSYN_0.6 | 5.5 | 352 ± 2.8 |
| HSM_LSYN_1.0 | 5.5 | 343 ± 3.1 |
| HSM_SF_0.6 | 5.0 | 337 ± 2.6 |
| HSM_SF_0.8 | 7.0 | 333 ± 3.0 |
| HSMFA_SSYN_0.6 | 4.4 | 348 ± 2.1 |
| HSMFA SSYN_1.0 | 5.0 | 341 ± 1.7 |
| HSMFA_LSYN_0.6 | 5.0 | 332 ± 3.6 |
| HSMFA_LSYN_1.0 | 5.5 | 342 ± 2.9 |
| HSMFA_SF_0.6 | 5.5 | 338 ± 1.8 |
| HSMFA_SF_0.8 | 7.0 | 334 ± 2.6 |

An electromechanical Zwick testing machine of 250 kN load cell was utilised in the flexural experiment. A 0.5 mm/min loading rate was applied to a prism measuring 40 x 40 x 160 mm. The specimens were notched ($\frac{d}{4}$) at the midspan to control the cracks opening, as in Figure 4.

**Figure 4.** The flexural strength test.

## 2.1 Digital image correlation (DIC) set-up

A unique pattern of random speckles or dots was applied to the specimen's surface (Point of interest) to prepare for the testing. These speckles were created by spraying black paint onto the white background of the specimen's surface, as in Figure 5.

**Figure 5: T**he speckles-patterned

The digital images of the test specimens under loading were captured using a CANON-5D Mark IV camera, with the key parameters outlined in Table 5. Increasing the camera's resolution can improve measurement accuracy since the displacement errors are typically small fractions of pixels. In this particular test, a camera with a resolution of 6720x4480 pixels and a standard 70 mm focal length is used, representing a notably higher resolution than the camera resolution used in previous work of Jaroslaw in 2019 [3]. The camera was mounted on a tripod, and weight was connected throughout the test to ensure stability. Throughout the experiment, the camera's optical axis remained perpendicular to the specimen's SOI, and no changes were made to the exposure and other parameters. The camera's sensor sensitivity was also tweaked to provide adequate photo brightness while minimising noise production. All camera settings were kept manually to preserve consistency and prevent alterations throughout the test (Figure 6); the camera was managed remotely through Wi-Fi to prevent the settings' interruption.

Out-of-plane motion is not expected to be an issue in this testing, but the effect of any out-of-plane movement. A weight was connected to the tripod throughout the test to ensure stability. Nevertheless, the camera was fixed 0.48 m from the specimen surface, as recommended by[35]. The external light was aimed at the specific area of interest to improve the image quality. The consistency of the specimen's surface texture remained unchanged, as the concrete surface displayed a random distribution of colour intensity and a satisfying diversity in its surface texture [36]. A continuous video was recorded for each sample at 25 frames per second (fps), generating significant data for DIC research. Using the VLC media player, each movie was turned into a photo at a rate of one image every two seconds to help with the process. The free XnViewMP software [37] transformed these photos into grayscale to decrease noise. The displacements were analysed in ascending numerical order, and the greyscale images were finally uploaded using GOM correlate 2D software [38]. GOM Correlate 2D is a free 2D DIC software that can measure full-field in-plane displacements and strains using the proper tools, including virtual extensometers, deviation labels, and distance variation.

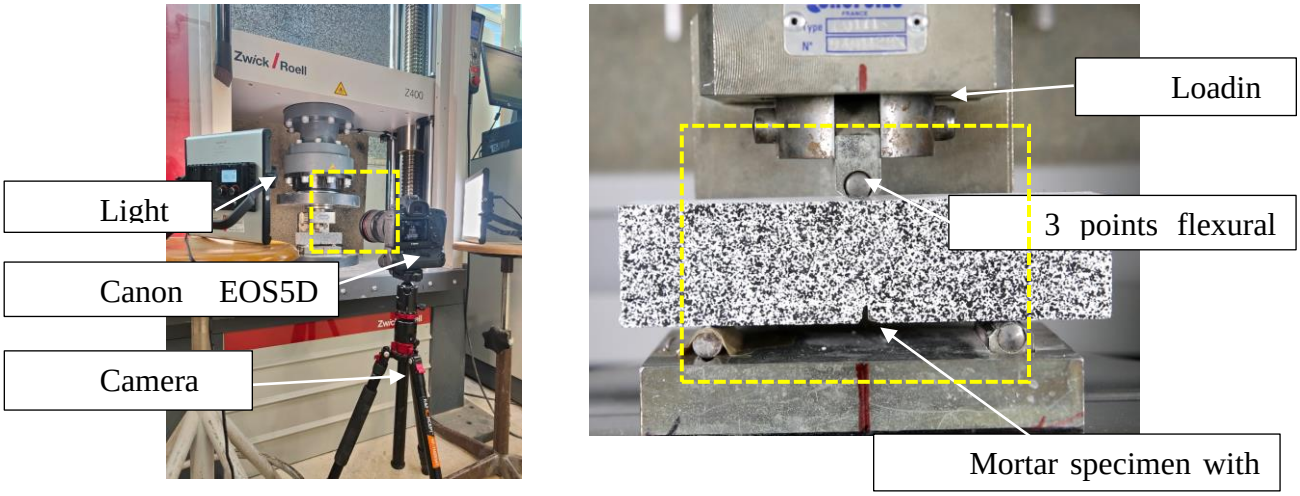


**Figure 6.** Experimental set-up of deformation measurement.

**Table 5.** Camera and lens specification

| | |
|---|---|
| Width of sensor | 6720 pixels |
| Height of sensor | 4480 pixels |
| Image sensor | CMOS |
| Manufacturer | Canon |
| Model | 5D EOS Mark IV |
| Mounted lens | Canon E.F. 24-70mm f/2.8 II USM |
| Colour display | sRGB |
| Shutter speed | 1/50s |
| Aperture | f/2.8 |
| Focal length | 70mm |
| Exposure time | 1/4000s |
| ISO speed | 800 |

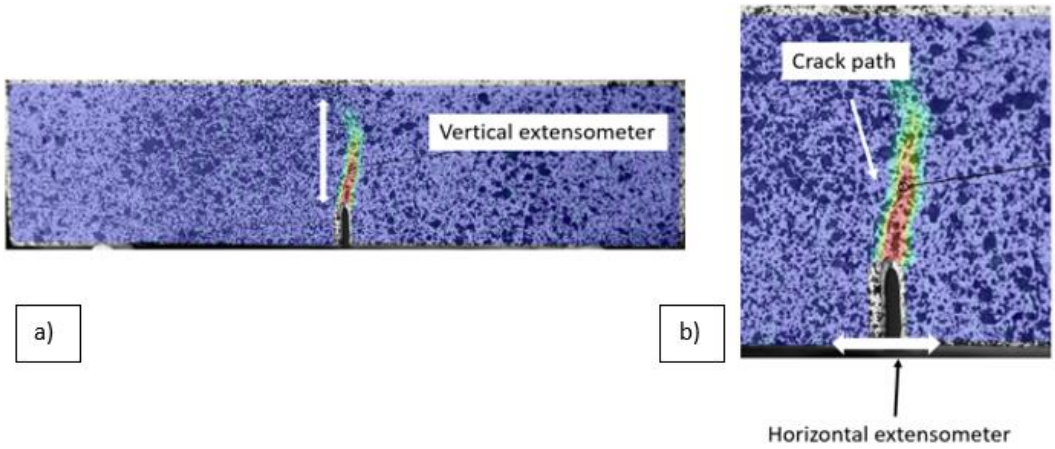


**Figure 7.** Strain visualisation on a flexural test specimen.

## 3 RESULTS AND DISCUSSION

### 3.1 Post-processing

Image processing was done using GOM correlate 2D [25], a free 2D DIC software capable of measuring full-field deflections of in-plane motion. In GOM, captured motion is divided into subsets, and all subsets have a different random pattern achieved by the stochastic pattern. In order to enable a comparison between DIC and machine results, 25 mm virtual extensometers were defined at different positions on the y-axis surface of interest (SOI). The results of the extensometers were compared to the measurements of the machine deflection (Δ) as tested. (Figure 7a). The same procedure was repeated on the x-axis for the (C-MOD).

### 3.2 Comparison of DIC and Machine Test Deflection

The behaviour of the prism samples with pre-made notches, having dimensions of 40 x 40 x 160, was assessed using GOM software and the Digital Image Correlation (DIC) technique. GOM software allowed for the placement of numerical extensometers in various directions, enabling the observation of strain variations on the surface of interest (SOI), as depicted in Figure 7. Moreover, the software facilitated identifying the crack propagation path before it became visible to the naked eye. When the bottom fibre of the cross-section reaches its tensile strength, the tested material displays a softening behaviour characterised by a decrease in resistance, an increase in deflection, and an expansion of the crack opening. The Force (F) vs. deflection (Δ) curves obtained from the testing machine and those generated through DIC using a numerical vertical extensometer positioned in the middle of the examined specimens are presented in Figures 8 (i) for the steel fibred mortars, 8 (ii) for the short synthetic fibred mortars, and 8 (ii) for the long synthetic fibred mortars respectively.

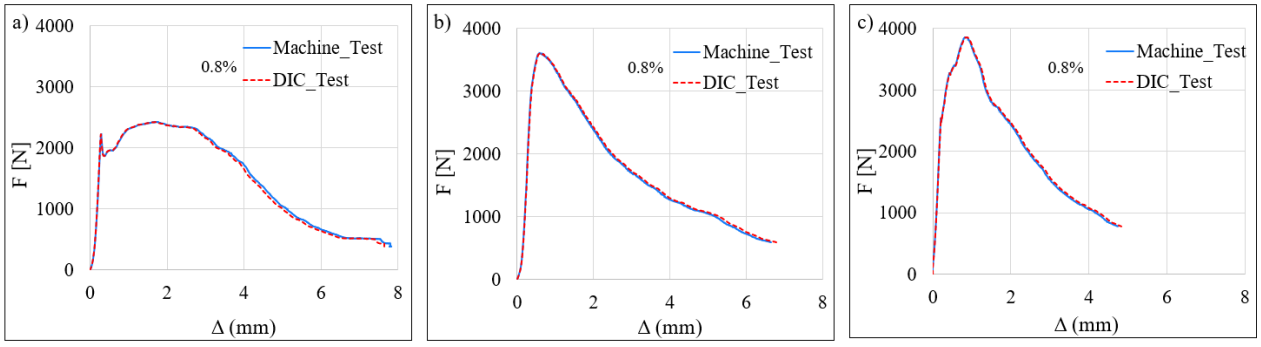


i) Steel Fibre

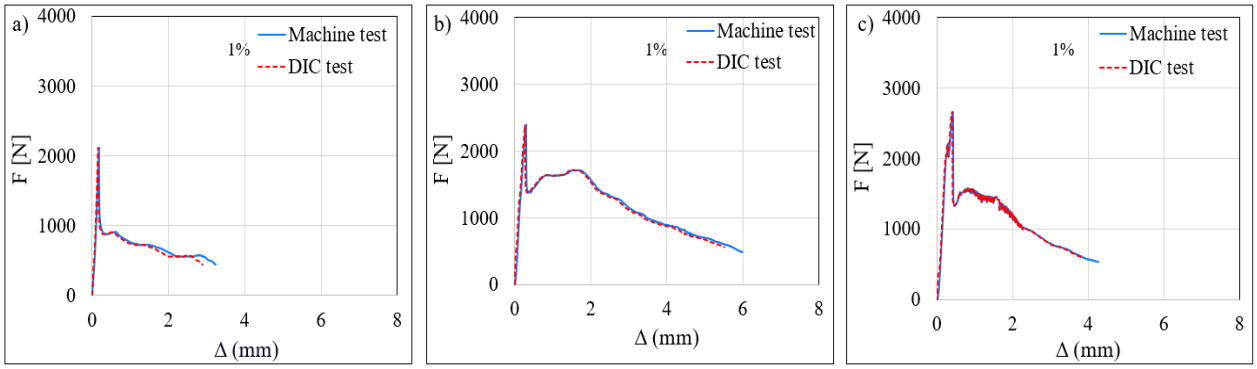


ii) Short synthetic Fibre

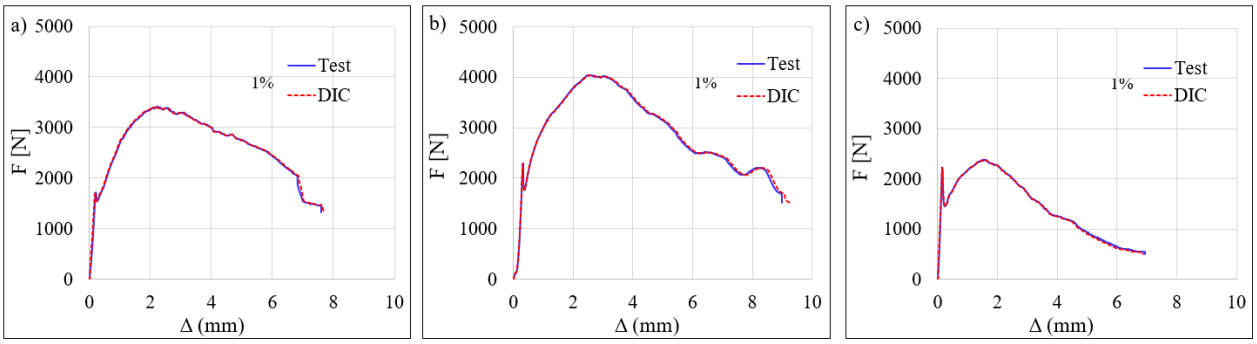


iii) Long synthetic fibre

**Figure 8.** Compare the machine and DIC-obtained load-deflection curves of different fibre-reinforced mortars of a) NSM, b) HSM, and c) HSMFA.

### 3.3 Crack Mouth Opening Displacement (CMOD)

The strong correlation between the results validates the effectiveness of the DIC technique in monitoring deformations in the tested samples. Additionally, horizontal extensometers placed at the base of the notch are utilised to measure the crack opening, referred to as Crack Mouth Opening Displacement (CMOD), as depicted in Figure 7 b, until the point of failure. This combined approach of DIC and CMOD measurements enhances understanding of the material's response to applied loads and provides valuable data for further analysis.

This behaviour was characterised by a decrease in resistance and an increase in deflection and crack opening. Figure 8 depicts the force-deflection curves obtained from the testing machine and the DIC technique, which employed a numerical vertical extensometer in the middle of the analysed specimens. The results obtained from the testing machine and the DIC technique exhibited a strong correlation, indicating the reliability and accuracy of the DIC method in monitoring deformations within the tested samples. This correlation confirmed the effectiveness of the DIC technique in capturing and analysing deformations within the specimens. Furthermore, horizontal extensometers were strategically placed at the base of the notch to measure the crack opening, referred to as Crack Mouth Opening Displacement (CMOD), until the point of failure (Figure 7 b). This measurement provided crucial insights into crack propagation and the material's fracture behaviour. The combination of CMOD measurements and the DIC technique enhanced the understanding of the material's response to applied loads and generated valuable data for further analysis. The reliable correlation between the testing machine and the DIC technique affirmed the usefulness of DIC as a reliable tool for monitoring sample deformations; the measurement of CMOD through horizontal extensometers allowed for a comprehensive analysis of crack behaviour and propagation as depicted in Figures 9 (i) for the steel fibred mortars, 9 (ii) for the short synthetic fibred mortars, and 9 (ii) for the long synthetic fibred mortars respectively.

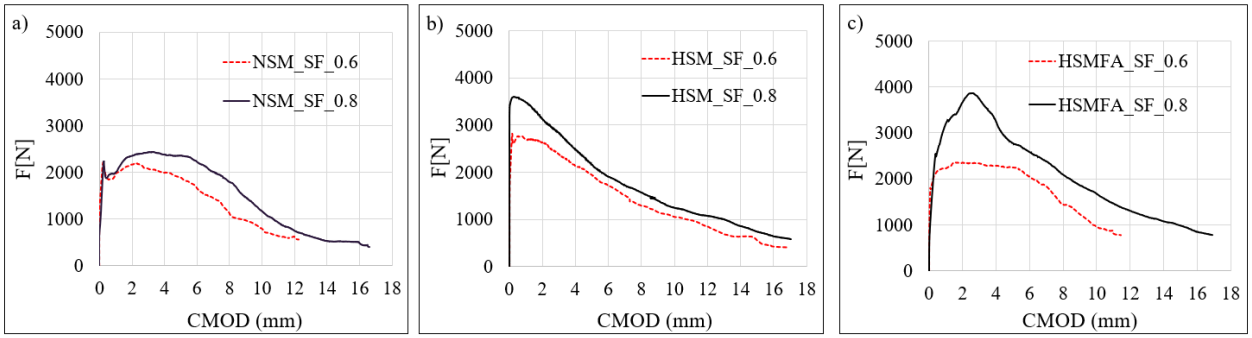


i) Steel Fibre

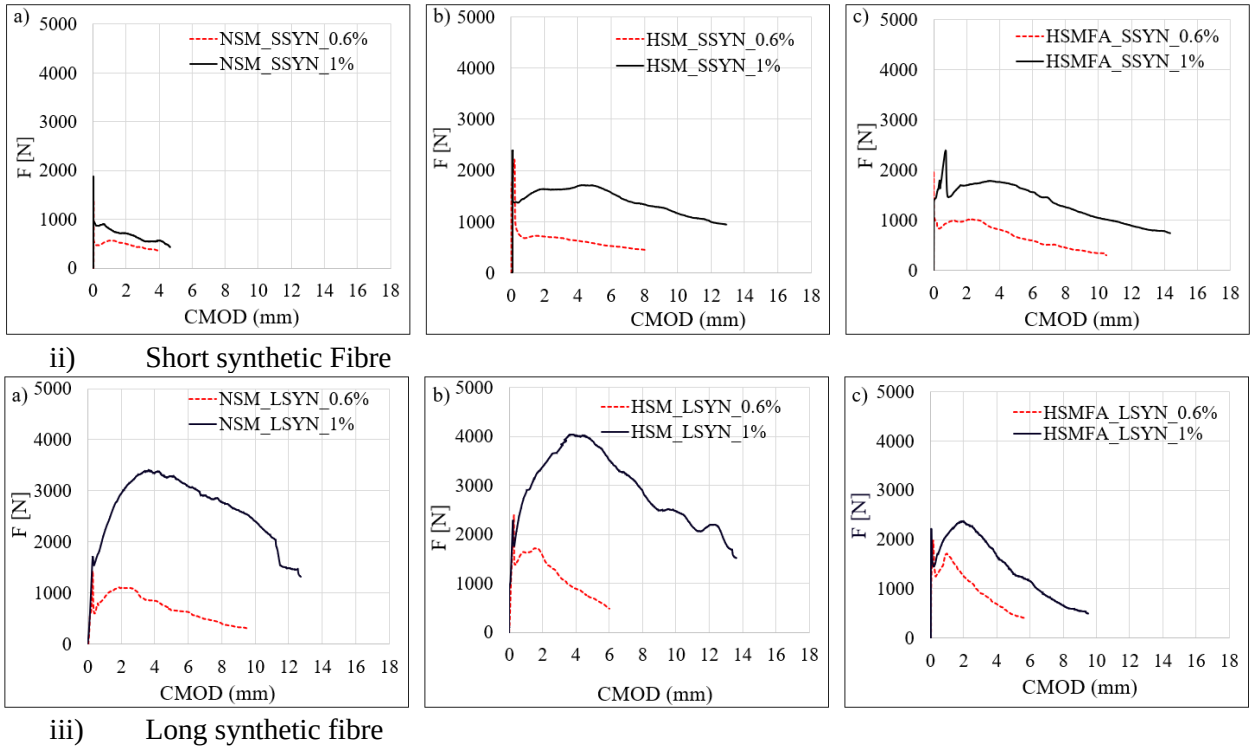


**Figure 9.** The DIC-obtained load-CMOD curves of different fibre-reinforced mortars of a) NSM, b) HSM, and c) HSMFA.

## 4 CONCLUSION

This study investigated the reliability of digital image correlation techniques for determining material deformations/displacement by comparison of the DIC and mechanical test methods for the fibre-reinforced mortars made from different fibres (steel, short synthetic, and long synthetic).

The study drew the following conclusions:

- Micro steel fibre exhibited remarkable performance of post-cracking behaviour; the strength increased with the fibre dosage.
- Synthetic fibres (polypropylene) exhibited remarkable performance in terms of post-cracking behaviour. Long synthetic fibres were identified as a promising alternative to steel reinforcement, with hardening properties at 1% fibre dosage.
- The digital image correlation technique proved useful in understanding the structure's material deformations/displacement and the cracking mechanism (CMOD).

## REFERENCES

1. Bello, G. Wardeh, B. González-Fonteboa, F. Martínez-Abella, Strain measurement of construction materials with digital image correlation, in Fib Symposium of Concrete Structures: New Trends for Eco-Efficiency and Performance, International Federation for Structural Concrete (fib) Portugal, 2021: pp. 1529–1538.

2. B. Pan, K. Qian, H. Xie, A. Asundi, Two-dimensional digital image correlation for in-plane displacement and strain measurement: A review, Meas Sci Technol. 20 (2009). https://doi.org/10.1088/0957-0233/20/6/062001.
3. Gorszczyk Jaroslaw, Malicki Konrad, Zych Teresa, Application of Digital Image Correlation (DIC) Method for Road Material T, Materials. (2019).
4. W.H. Peters, W.F. Ranson, Digital imaging techniques in experimental stress analysis, 1982. http://spiedl.org/terms.
5. H. Schreier, J.J. Orteu, M.A. Sutton, Image correlation for shape, motion and deformation measurements: Basic concepts, theory and applications, Springer US, 2009. https://doi.org/10.1007/978-0-387-78747-3.
6. T.C. Chu, W.F. Ranson, M.A. Sutton, Applications of digital-image-correlation techniques to experimental mechanics, Exp Mech. 25 (1985) 232–244. https://doi.org/10.1007/BF02325092.
7. S. Dai, X. Liu, K. Nawnit, Experimental study on the fracture process zone characteristics in concrete utilising DIC and AE methods, Applied Sciences (Switzerland). 9 (2019). https://doi.org/10.3390/app9071346.
8. M. Hagara, R. Huňady, P. Lengvarský, J. Bocko, Numerical Verification of a Full-field Deformation Analysis of a Specimen Loaded by Combined Loading, American Journal of Mechanical Engineering. 2 (2014) 307–311. https://doi.org/10.12691/ajme-2-7-29.
9. M. Pellet, A. Chenel, M. Behr, L. Thollon, Is digital image correlation able to detect any mechanical effect of cranial osteopathic manipulation? – A preliminary study, International Journal of Osteopathic Medicine. 29 (2018) 10–14. https://doi.org/10.1016/j.ijosm.2018.07.004.
10. Online, Guide at digitalimagecorrelation.org, (2023).
11. G. Wardeh, E. Ghorbel, Prediction of fracture parameters and strain-softening behaviour of concrete: effect of frost action, Materials and Structures/Materiaux et Constructions. 48 (2015) 123–138. https://doi.org/10.1617/s11527-013-0172-8.
12. A.B. Kizilkanat, N. Kabay, V. Akyüncü, S. Chowdhury, A.H. Akça, Mechanical properties and fracture behaviour of basalt and glass fibre reinforced concrete: An experimental study, Constr Build Mater. 100 (2015) 218–224. https://doi.org/10.1016/j.conbuildmat.2015.10.006.
13. S.M.S. Kazmi, M.J. Munir, Y.F. Wu, I. Patnaikuni, Effect of macro-synthetic fibres on the fracture energy and mechanical behaviour of recycled aggregate concrete, Constr Build Mater. 189 (2018) 857–868. https://doi.org/10.1016/j.conbuildmat.2018.08.161.
14. N. Banthia, R. Gupta, Influence of polypropylene fibre geometry on plastic shrinkage cracking in concrete, Cem Concr Res. 36 (2006) 1263–1267. https://doi.org/10.1016/j.cemconres.2006.01.010.
15. M.K. Kazberuk, Post-cracking behaviour and fracture energy of synthetic fibre reinforced concrete, Medziagotyra. 22 (2016) 542–547. https://doi.org/10.5755/j01.ms.22.4.13246.
16. A.G. Kooiman, C. Van Der Veen, J.C. Walraven, Modelling steel fibre-reinforced concrete post-cracking behaviour for structural design purposes, HERON-ENGLISH EDITION-. 45 (2000) 275–308.
17. D.S. Aliyu, H. Ibrahim, H. Hamza, COMPARATIVE STUDY OF ELASTIC AND PLASTIC ANALYSIS OF INDIAN STEEL MEMBERS SUBJECTED TO FIRE USING SAFIR AND ANSYS SOFTWARE, International Conference. (2015).
18. H. Ibrahim, D.S. Aliyu, H. Hamza, Vibration Control of A-Frames Structure Using Tuned Mass Damper, in Second International Conference Technology and Management, Issue-July, Pp-873-884, 2015.
19. A.C. 440, ACI 440.1R-03. Guide for the design and construction of concrete reinforced with FRP bars, American Concrete Institute (ACI), Farmington Hills, Mich., USA. (2015) 42pp.
20. V.S. Vairagade, K.S. Kene, Introduction to Steel Fiber Reinforced Concrete on Engineering Performance of Concrete, International Journal of Scientific & Technology Research. 1 (2012) 4–6.
21. H. Ibrahim, D.S. Aliyu, A. Ma'aruf, M. Farouq, Ground-borne vibration transmission on structure (effect and control): A review, International Journal of Engineering and Science Research. 1 (2018) 1–7.

22. S. Yin, R. Tuladhar, F. Shi, M. Combe, T. Collister, N. Sivakugan, Use of macro plastic fibres in concrete: A review, Constr Build Mater. 93 (2015) 180–188. https://doi.org/10.1016/j.conbuildmat.2015.05.105.
23. J. Xie, Z. Zhang, Z. Lu, M. Sun, Coupling effects of silica fume and steel-fiber on the compressive behaviour of recycled aggregate concrete after exposure to elevated temperature, Constr Build Mater. 184 (2018) 752–764. https://doi.org/10.1016/j.conbuildmat.2018.07.035.
24. J. Xie, J. Li, Z. Lu, Z. Li, C. Fang, L. Huang, L. Li, Combination effects of rubber and silica fume on the fracture behaviour of steel-fibre recycled aggregate concrete, Constr Build Mater. 203 (2019) 164–173. https://doi.org/10.1016/j.conbuildmat.2019.01.094.
25. GOM, GOM Correlate. Software for 3D Testing Data, (2019).
26. J. Zhao, Y. Sang, F. Duan, The state of the art of two-dimensional digital image correlation computational method, Engineering Reports. 1 (2019) e12038. https://doi.org/https://doi.org/10.1002/eng2.12038.
27. B. Pan, K. Qian, H. Xie, A. Asundi, Two-dimensional digital image correlation for in-plane displacement and strain measurement: a review, Meas Sci Technol. 20 (2009) 62001. https://doi.org/10.1088/0957-0233/20/6/062001.
28. Michael A. Sutton, Jean-José Orteu, Hubert W. Schreier, Image Correlation for Shape, Motion and Deformation Measurements. Basic Concepts, Theory and Applications, Springer, 2009. https://doi.org/10.1007/978-0-387-78747-3.
29. M.-H. SHIH, W.-P. SUNG, Application of digital image correlation method for analysing crack variation of reinforced concrete beams, Sadhana. 38 (2013) 723–741. https://doi.org/10.1007/s12046-013-0141-5.
30. Fridtjov Irgens, Continuum Mechanics, Springer, 2008.
31. S. Choi, S.P. Shah, Measurement of deformations on concrete subjected to compression using image correlation, Exp Mech. 37 (1997) 307–313. https://doi.org/10.1007/BF02317423.
32. S. Xiang, L. Zeng, J. Zhang, J. Chen, Y. Liu, G. Cheng, J. Mo, A DIC-Based Study on Compressive Responses of Concrete after Exposure to Elevated Temperatures, Materials . 12 (2019). https://doi.org/10.3390/ma12132044.
33. NF EN 197-1, European standard on composition, specification, and conformity criteria for common cement, 2012.
34. NF EN 934-2, European standard on admixture for concrete, mortar, and grout, 2012.
35. Neil A Hoult, W. Andy Take, Chris Lee, Michael Dutton, Experimental accuracy of two-dimensional strain measurements using Digital Image Correlation _ Elsevier Enhanced Reader, Journal of Engineering Structure. (2013).
36. TM Fayyad, J.M. Lees, Application of Digital Image Correlation to Reinforced Concrete Fracture, Procedia Materials Science. 3 (2014) 1585–1590. https://doi.org/10.1016/j.mspro.2014.06.256.
37. P. Gougelet, XnView MP Windows, (2021).
38. GOM, GOM Correlate. Software for 3D Testing Data, (2019).